GROWTH CHARACTERIZATION OF RF MAGNETRON SPUTTERED $BiFeO_3$ ON EPITAXIAL $SrTiO_3$

THESIS

Presented to the Graduate Council of
Texas State University-San Marcos
in Partial Fulfillment
of the Requirements

for the Degree

Master of SCIENCE

by

Rye A. Johnson, B.S.

San Marcos, Texas
May 2013

GROWTH CHARACTERIZATION OF RF MAGNETRON SPUTTERED

$BiFeO_3$ ON EPITAXIAL $SrTiO_3$

Committee Members Approved:

_____
Gregory F. Spencer, Chair

_____
Ravi Droopad

_____
Wilhelmus J. Geerts

Approved:

_____
J. Michael Willoughby
Dean of the Graduate College

FAIR USE AND AUTHOR'S PERMISSION STATEMENT

Fair Use

Duplication Permission

ACKNOWLEDGEMENTS

I would first like to thank all the people that work really hard behind the scenes of the physics department that don't usually get the appreciation they deserve. A special thanks to Leandra and her office staff for keeping the department in line and getting us paid. Nelson Koeck, you kept us safe and always made me laugh.

Thanks Mom and Dad for your endless support, financially and emotionally.

Anup K. Bandyopadhyay, you were always willing to assist me with my growths and measurements. Thank you to Eric for taking time from your very busy schedule for equipment training.

The offered ideas and advice from my committee members, Ravi Droopad and Wim Geerts, were greatly appreciated. Thanks, Ravi, for providing me with the samples I requested from your lab.

And of course, committee chair Greg Spencer, thank you for taking a chance and accepting me as your graduate research assistance.

Oh, and Kim too...

This manuscript was submitted on March 25, 2013.

TABLE OF CONTENTS

Page

LIST OF TABLES

Table **Page**

LIST OF FIGURES

Figure **Page**

ABSTRACT

GROWTH CHARACTERIZATION OF RF MAGNETRON SPUTTERED

$BiFeO_3$ ON EPITAXIAL $SrTiO_3$

by

Rye A. Johnson, B.S.

Texas State University-San Marcos

May 2013

SUPERVISING PROFESSOR: GREGORY F. SPENCER

$BiFeO_3$, or BFO, is a multiferroic material that exhibits the simultaneous appearance of ferroelectric and antiferromagnetic properties. What makes this material unique is its ability to display this property at room temperature, making it of great practical interest for device application. We report on our synthesis and growth characterization of thin BFO films by RF magnetron sputtering on epitaxial $SrTiO_3$/Si substrate grown at Texas State University-San Marcos. The resulting polycrystalline thin films, ranging from ~ 100 to 600nm, were characterized by x-ray diffraction for crystallinity and EDS for film composition. We also measured the temperature dependent magnetic characterization by vibrating sample magnetometer between 4.2K

and 300K. Imaging by scanning electron and atomic force microscopy was performed to study spontaneously formed thin film morphology.

CHAPTER 1

INTRODUCTION

Ferroics is the general term for the study of ferromagnets, ferroelectrics, and ferroelastics. As an example, ferromagnetism is the mechanism that provides certain materials, such as iron, with the ability to form permanent magnets. These ferromagnetic materials are important and are the basis for many devises such as electric motors, transformers, and magnetic storage. [1]

Multiferroic materials are defined as those that demonstrate more than one primary ferroic parameter in a single phase, but can be expanded to include non-primary parameters such as antiferromagnetism. Typical multiferroics of interest are part of the perovskite structure, more specifically, the perovskite transition metal oxides. These materials have a general chemical formula represented as ABO_3. Here A represents large ions like alkali or rare earth metals and the B ions can be transitional metals. [2]

Bismuth ferrite, $BiFeO_3$ or BFO, is reported to be of the rhombohedrally distorted ferroelectric perovskite with G-type antiferromagnetism (T_N ~ 643K). [3] [4] [5] As a result, an electric field can induce change in magnetization, and an external magnetic field can induce electric polarization. What makes BFO unique is its ability of demonstrating this capability at room temperature. This makes BFO one of the leading candidates for device applications. Multiferroics show potential for application in actuators, switches, or magnetic field sensors and also show promise for application in future magnetic storage and spintronic devices.

The goal for this thesis is to establish a methodology for optimizing BFO synthesis using sputter deposition by utilizing a number of thin film characterization techniques. Creating a reproducible procedure for growth and consistent characterization results with available equipment at Texas State will provide the groundwork for future research opportunities. As described previously, multiferroic research has been and is still a growing field of interest which will provide this university with many more years of prospective research.

Part of the content of this thesis was presented in a poster session at the 2013 Texas sections joint meeting at Tarleton State University in Stephenville, Texas.

CHAPTER 2

CHARACTERIZATION TECHNIQUES

This chapter will provide a basic review of various measurement techniques used that were used to characterize the $BiFeO_3$ I made. The primary characterization methods used during the research included x-ray diffraction (XRD), vibrating sample magnetron (VSM), scanning electron microscope (SEM), and atomic force microscopy (AFM). Each of these instruments will be discussed with additional used measurement methods available on the tools.

X-ray Crystallography

A crystal is a three-dimensional periodic array of some unit of atoms or molecules. [6] Bragg diffraction was first proposed by William Lawrence Bragg and William Henry Bragg in 1913 in response to their discovery that crystalline solids produced patterns of reflected x-ray. This discovery won them the Nobel Prize in 1915. [7] They found that their sample crystals, at certain specific wavelengths and incident angles, produced intense peaks of reflected radiation known as Bragg peaks. The conditions for these scattered radiation peaks are: 1) the x-rays should be specularly reflected in any one atom plane and 2) the reflected rays of consecutive atom planes should constructively interfere. These two conditions lead to the Bragg condition:

$$n\,\lambda = 2\,d\,sin\theta$$

Fig. 1 shows a representation of incident rays interacting with the different crystal planes where *d* is the distance between atomic planes, θ is the angle of incidence from the

sample surface, and *n* is an integer giving the diffraction order. Since the details of the diffraction pattern are due to the specific nature of the crystal, diffraction can be used to determine the crystal structure [8].

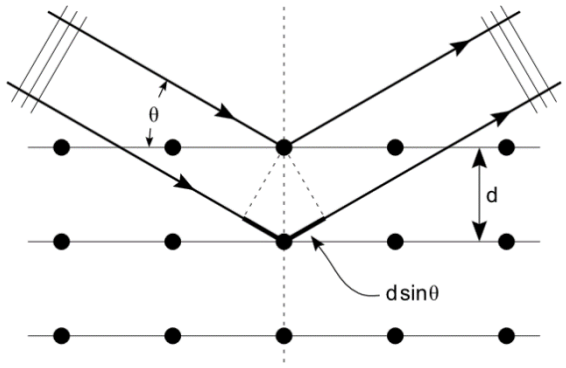

Figure 1. Representation of Reflected X-rays in a Crystal.

X-ray Diffraction

X-ray diffraction, or XRD, uses a known high energy x-ray wavelength to determine the crystal structure from the measured diffraction pattern by using the Bragg conditions described above. The XRD used was the Bede D1 X-ray system as shown in Fig. 2. To produce x-rays of specific energies, a heated filament produces an electron beam which is accelerated and then directed at a copper disk named the target. Upon collision with the target, the electrons emit EM-radiation or transfer their energy to copper atoms in the target. The transferred energy to the copper atoms by the electron beam is used to excite copper atoms into a higher energy state. These excited atoms then relax back to ground state and there by release the energy shell difference in the form of an x-ray photon. These intense x-rays are monochromatic and are then passed through a filter for specific $K\alpha$ x-ray energies to remove higher order absorptions peaks.

The sample is attached with double side tape onto a microscope slide that is attached to the aluminum sample stage and mounted in the system. This microscope

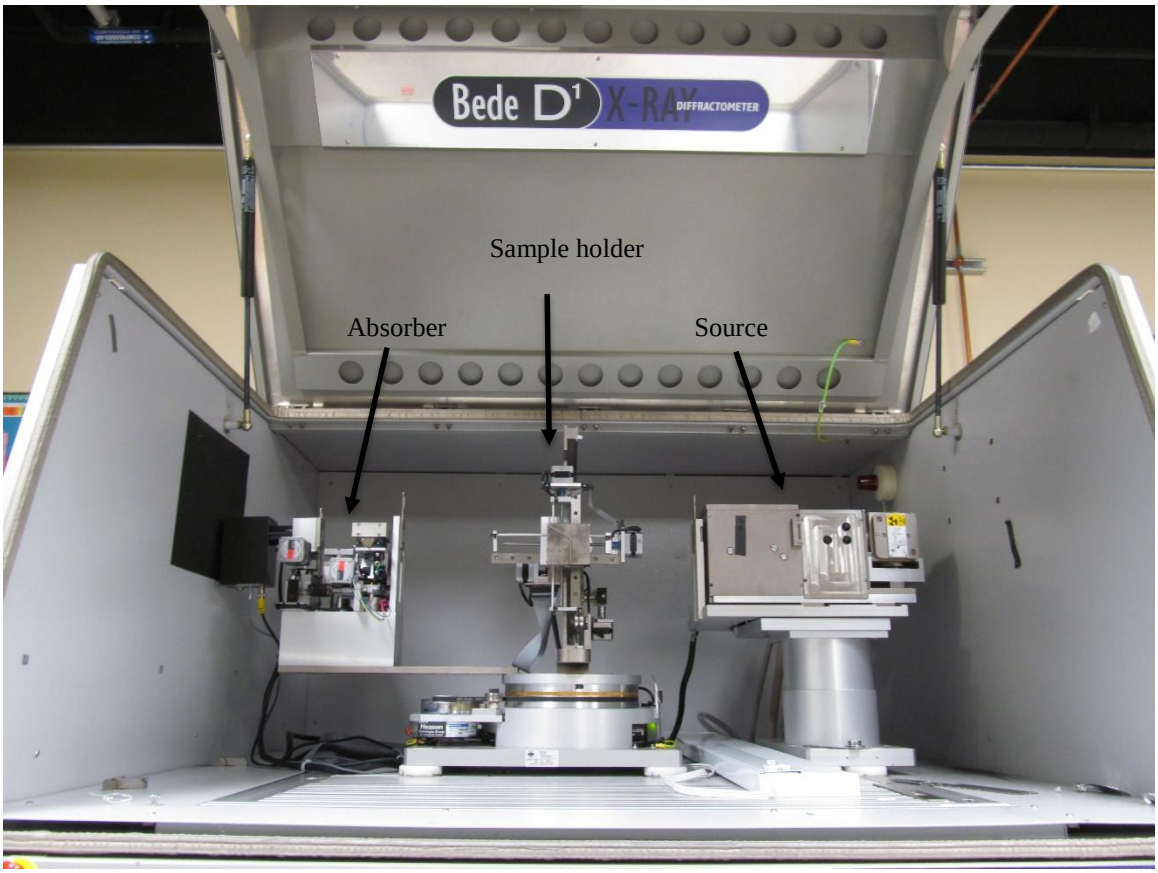

Figure 2. Bede D1 X-ray System. Absorber, sample stage, and x-ray source all under open radiation hood.

slide helps prevent the measurement of the aluminum sample holder. The radiation hood is closed and proper alignment techniques are used to center the sample to give a glancing incidence in the x-ray beam. The sample is then run through a standard θ-2θ measurement. This measurement requires the x-ray source and detector be the same distance from the sample holder. The Bede D1 system is set up so that as the sample holder sweeps through the designated angle θ, the detector will rotate at 2θ. As the incident angle θ is varied under computer control, the diffraction condition changes, giving rise to x-ray peaks at particular values of θ. As the θ-2θ scan is taken, the diffraction pattern is displayed as a graph of x-ray signal (in counts per second) versus the 2θ angle. After the scan is finished, a smoothing option can then be selected to

reduce any noise. This graph can then be compared to the International Centre for Diffraction Data [9] (ICDD) of available experimental 2θ data measured by others to identify the diffraction peaks with crystallographic planes.

Physical Properties Measurement System

The Physical Property Measurement System, or PPMS, housed at Texas State is a high magnetic field, variable temperature measurement platform made by Quantum Design. This system is built around a 9 tesla superconducting magnet. It contains a sealed EverCool sample chamber supported by a CSW-71 helium compressor unit designed by Sumitomo Heavy Industries Ltd. The temperature control for the closed helium system is controlled by the PPMS model 6000 controller with temperature range

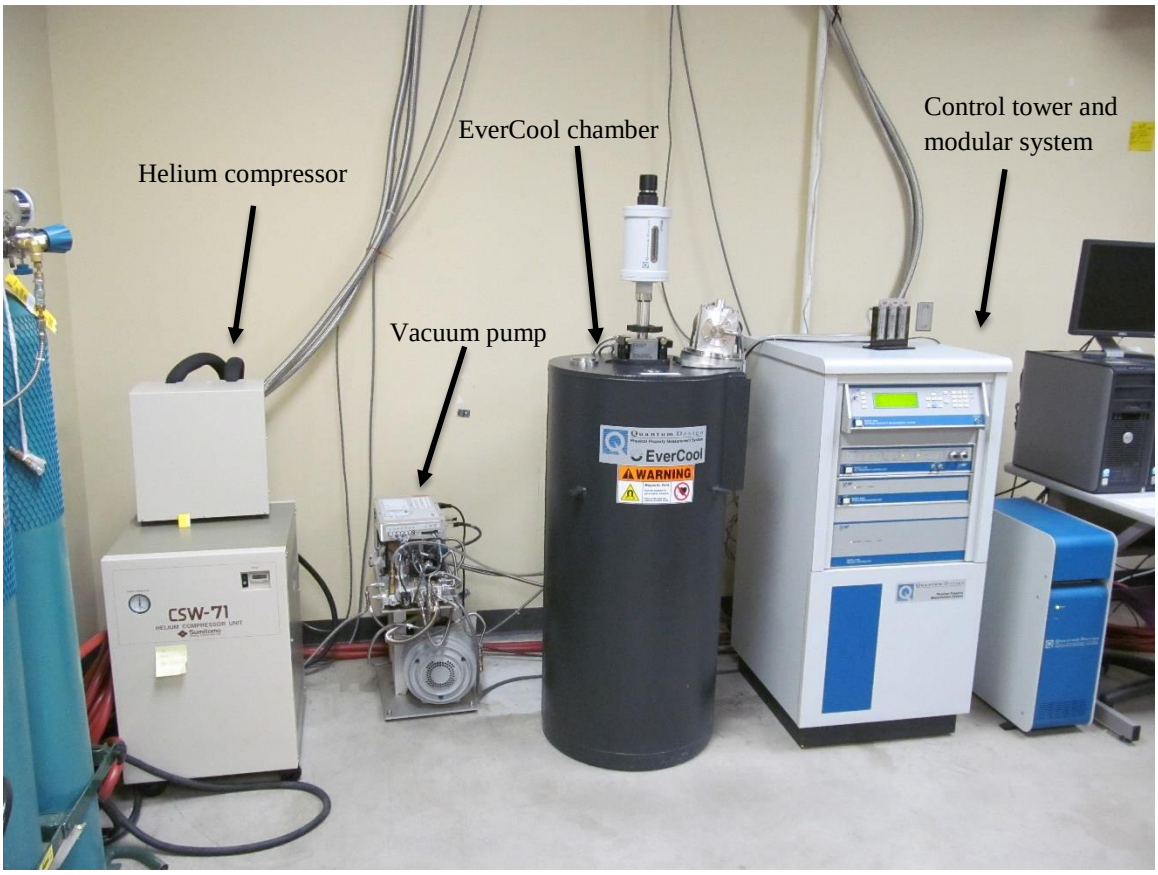

Figure 3. PPMS. Sumitomo helium compressor unit, Vacuum pump, Quantum Design EverCool chamber with attached VSM head, Quantum Design PPMS control tower and modular control system.

of 1.9K to about 320K. Also included in the PPMS tower are the Model 6700 Magnet controller with a -9T to 9T field, the Model 7100 AC transport controller, and the Model 6500 PPMS options controller. These systems are shown in Fig. 3. The system comes with various measurement inserts including a Vibrating Sample Magnetometer (VSM).

PPMS Vibrating Sample Magnetometer

The Vibrating Sample Magnetometer (VSM) was used to measure the magnetic properties of the various BFO samples. The VSM measurement is accomplished by oscillating the sample, with the model P525 VSM head shown in Figure 4, near a pick up coil and synchronously detecting the voltage induced in the pickup coils. By using a compact gradiometer pickup coil setup, a relatively large oscillation amplitude (about 1-

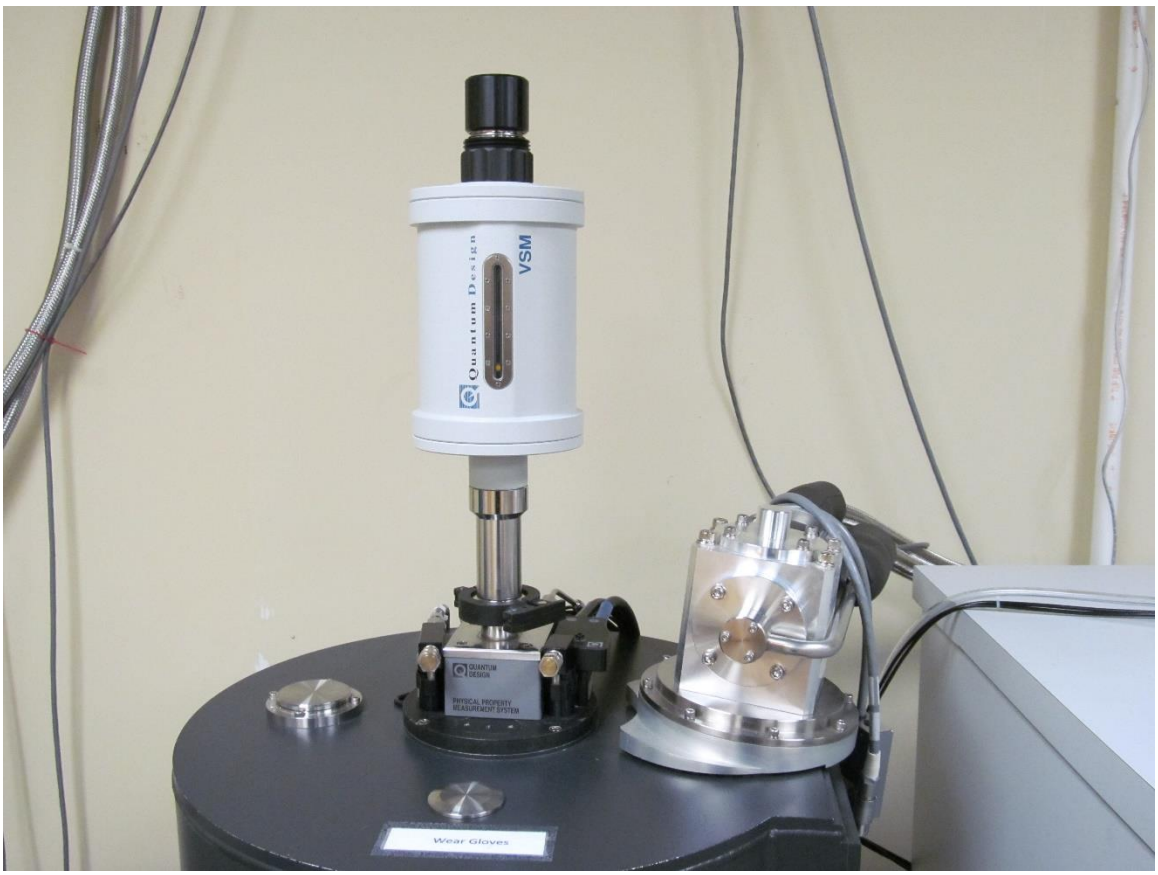

Figure 4. Quantum Design VSM Head.

3mm) and a frequency of 40 Hz, the system is able to resolve magnetization changes of less than 10^{-6} emu. [10]

Samples for measurement are typically 2-3mm square cleaved from a larger thin film sample. These samples are attached to a quartz VSM sample holder. The quartz sample holder is then attached to the VSM rod. A rod guide is inserted into the EverCool chamber and the VSM head is placed on top as shown in Figure 4. The VSM rod with attached sample is then inserted through the top of the VSM head and into the EverCool chamber. From the computer control interface, the VSM port is selected and activated for use. Then a system purge is done to flush the sample chamber of contaminants. The VSM sample is then run through a centering process to center the BFO sample in the coil pickups. Once centered, a VSM run can be created or a previously saved script can be used. A wide variety of measurement options are available for adjustment including: temperature, magnetic field, magnetic field sweep time, run time, hold time, etc. All of these options can be manipulated to create a VSM sample measurement depending on the user's requirements.

For the magnetic characterization of the BFO samples, a measurement file was created to measure the magnetic hysteresis curve. The magnetic hysteresis curve is the

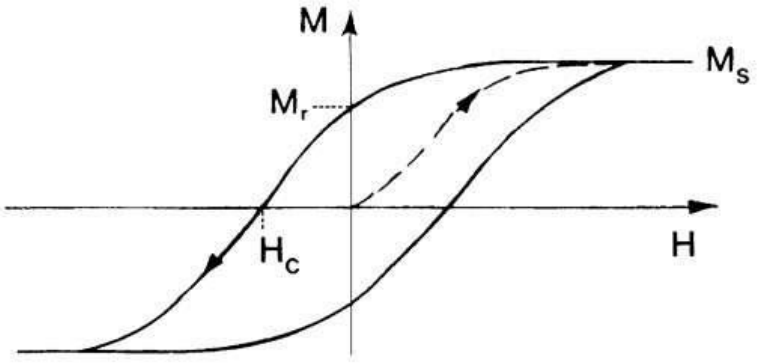

Figure 5. Theoretical Hysteresis Curve. Theoretical model of magnetization *M* and magnetic field *H*.

relation between the applied magnetic field and the magnetic moment of the material. Fig. 5 shows an example of a ferromagnetic material.

Starting from the origin, the initial field and moment are zero representing a non-magnetized material in the VSM with no initial magnetic field. As the applied magnetic field rises, the magnetization of the material also rises to a saturation point (M_s). As the magnetic field returns to zero, the magnetization reaches a remanence (M_r). This is the materials magnetization after the magnetic field hits saturation and returns to zero. As the magnetic field moves toward the negative field, the magnetization remains positive until coercivity (H_c). This position represents the amount of opposing magnetic field required to return the materials magnetization to zero. These values provide valuable ferromagnetic information about the material that can be used for device application.

Scanning Electron Microscope

A standard optical microscope uses lenses to focus visible light to magnify small objects. The resolving power of an optical microscope depends on the numerical aperture of the objective and the wavelength of the used light and is typically about half the wavelength of the light used, i.e. around 300nm. In order to resolve smaller features, other techniques need to be used such as AFM or electron microscopy. A scanning electron microscope uses a focused beam of electrons to create an image and can easily resolve details as small as 10nm.

Texas State recently acquired the Helios NanoLab 400 Dual Beam SEM as shown in Fig. 6. The sample is placed into a high vacuum chamber where a tungsten filament produces the electrons. The electrons beam is focused through a series of lenses in an ultra-high vacuum environment. These lenses act as traditional optical microscope lenses

Figure 6. Helios NanoLab 400 Dual Beam SEM.

but are quite different. The SEM column condenser lenses are electromagnetic lenses. They use a strong magnetic field to focus the beam of electrons. These lenses are used to focus the electron beam onto the surface of the sample. The focused beam is then scanned in a raster pattern across the surface of the sample. The incident electrons interact with the sample atoms in several ways. These interactions include the generation of backscattered primary electrons, secondary electron emission, and the emission of x-rays, all of which can used for imaging and/or chemical analysis. Backscattered electrons result from the high energy electrons produced by the SEM that are elastically reflected from the sample surface. Secondary electrons are ejected electrons from the sample caused by the incident electron beam and x-ray emission is the result of an incident electron striking an electron from the sample, exciting it to a higher energy shell. As this

electron relaxes back to its original state, an x-ray may be emitted. All three of these effects are utilized to create a quality surface image on the nanometer scale. For further investigation of sample composition, the SEM at Texas State also supports energy-dispersive x-ray spectroscopy.

Energy-Dispersive X-ray Spectroscopy

Energy-dispersive x-ray spectroscopy, or EDX, is a technique used to analyze the elemental composition of a sample. Used in conjunction with the SEM, EDX can measure a very small spot on the sample or scan larger areas. This technique utilizes the SEM's electron beam by taking advantage of the incident surface interactions. EDX measures the previously described interaction of x-ray emission by excitation. Because each atom has a unique structure, these emitted x-rays can be interpreted to a unique spectrum. This spectrum provides elemental information and composition of the sample.

Atomic Force Microscope

Atomic force microscopy, or AFM, is a high resolution type of scanning probe that gathers topographical information by scanning a special tip across the surface of a sample. The advantage to this system over, say the SEM, is that while the SEM can provide a detailed 2-d image of the surface, the AFM provides a 3 dimensional profile of the surface. AFM allows us to see and measure surface features with unprecedented resolution and accuracy and almost any sample type can be imaged.[11]

The Digital Instruments, Veeco Metrology Group SPM model Dimension 3100 AFM, shown in Fig. 7, was used for further investigation of BFO surface structures. There are several working modes of the AFM for different needs. Tapping mode was used to study the BFO sample and is usually the most common and least damaging

method. Tapping mode AFM operates by scanning a special tip attached to the end of an oscillating cantilever across the sample surface. This intermittent contact method reduces surface damage. This special precision tip is designed with radius of curvature on the order of nanometers and attached on the end of the cantilever. The cantilever has a mirrored surface on the opposite side of the tip. The cantilever and tip are then mounted to the scanner and a laser is aligned onto the end of the mirrored side of the cantilever. The cantilever is oscillated at or slightly below its resonance frequency with a set amplitude. A sample is then placed on the AFM sample stage and held in place by a vacuum chuck. The sample stage is then rotated till the sample is under the scanner and cantilever tip. The tip is then brought into working distance from the surface. The tip is then scanned along the surface in a raster pattern in a desired size and area. The systems feedback loop maintains a constant oscillation amplitude by maintaining a constant RMS of the oscillation signal interpreted by the reflected laser from the oscillating cantilever. The vertical adjustments from the feedback loop are stored and interpreted as topographical information of the sample.

Figure 7. AFM. (top) AFM on isolation table with hood up and adjacent control systems. (bottom) Close up of AFM scanning and optics systems.

CHAPTER 3

BFO GROWTH METHOD

In this work, Bismuth ferrite ($BiFeO_3$, abbreviated as BFO) is RF magnetron sputtered on top of $SrTiO_3$//Si, or STO, which is epitaxially grown in the molecular beam epitaxy lab. These processes are all done on site at Texas State University-San Marcos. This process and ability at Texas State provides a unique opportunity for future research in terms of substrate variations and customization. This chapter will provide a detailed description of these processes.

Molecular Beam Epitaxy

Molecular beam epitaxy, or MBE, is an evaporation method that takes place in ultra-high vacuum (UHV). The UHV environment and high substrate temperature provides the ideal conditions for single crystal growth. One of the most significant advantages of MBE is the ability to incorporate UHV associated surface analyzing equipment directly into the preparation and growth chambers. This allows the chemical and structural properties to be monitored throughout the growth process. [12]

STO Growth

Described in the article by Ravi Droopad et al. [13] is a complete description for the growth process of the buffer layer STO//Si we used for BFO growth. The following provides a summary of growth procedure from the article.

The bare (100) oriented silicon substrate is first exposed to ozone in a commercial ultraviolet ozone generator to assist in the removal of surface carbon after removal of the native oxide layer. The native oxide is removed in-situ using a Sr-assisted desorption at approximately 800°C. The temperature is then lowered to the growth temperature which is in the range of 200-500°C. A seed layer of Sr is deposited, up to ½ monolayers, until an ideal surface reconstruction is observed by RHEED. Then the growth of strontium titanate is a co-deposition of Sr and Ti metal with an oxygen gas present. The STO used for this work was sample number 4-1016 with a thickness of about 200A STO//Si(100).

Magnetron Sputtering

RF magnetron sputtering is a type of physical vapor deposition method for depositing thin films. Plasma is ignited in an argon rich environment by applying a high voltage between the target and substrate. The advantage of the magnetron sputtering technique is the ability to concentrate the plasma around the target area by the use of strong magnetic fields generated by permanent magnets inserted under the target material of deposition guns. This concentrated plasma field produces a higher density of ions which provide an increased growth rate. In the use of a non-conducting target, an RF magnetron is used to prevent a charge buildup on the target surface. The ATC ORION 5 UHV series sputtering system from AJA International, Inc. was used for the sputtering process of BFO. Fig. 8 shows the ATC ORION 5 (or AJA) growth chamber with attached load lock and neighboring control tower. Inside the main chamber are 5 available sputtering sources set up in a sputter up design as depicted in Fig. 9. The sample holder utilizes a motorized rotating holder in front of a quartz lamp array

Figure 8. ATC ORION 5 UHV. From left to right, the AJA main sputtering chamber with attached load lock and adjacent control tower.

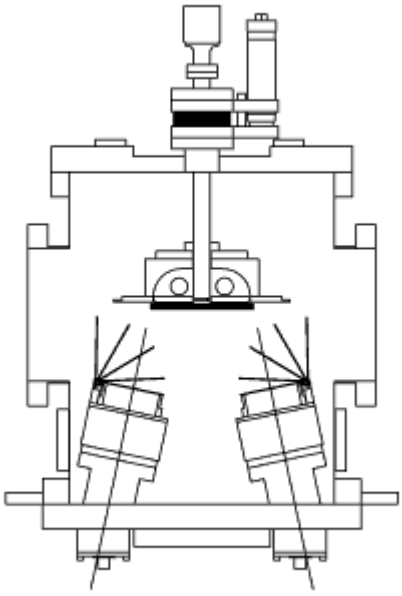

Figure 9. Main Chamber Sample Holder and Con-focal Source Diagram.

optimized for temperature and deposition uniformity. Also, the sources are oriented in con-focal geometry for an even higher degree of uniformity. The AJA is set up with two RF and three DC power supplies to be used for deposition dependent on material being sputtered (RF for nonconductors and DC for conductors). BFO sputtering is optimized for sputtering with the automatic matching 300 Watt RF generator.

Depositions start with a small sample, about 1cm x 1cm, cleaved from the previously grown STO//Si wafer (described above) placed on top of a 4" silicon pilot wafer attached to the sample holder. The prepared STO sample is then loaded into the main chamber via the load lock. The sample is then rotated and heated to an operating temperature of 600°C. Argon and oxygen are introduced into the system at a flow rate of 23 sccm and 12 sccm respectively. The plasma is then ignited in the main chamber at a 30% working power, or 90 Watt, with the magnetron shutter closed. This state is held for 5 minutes to clean the BFO target surface. This also allows for a stabilization of the temperature. After the 5 minutes of pre-sputtering, the BFO target shutter is opened and growth can begin with continued sample rotation for uniformity.

Previous growth tests using the Quartz Crystal Microbalance (QCM) were done to evaluate the BFO growth rate. The AJA at 30% power results in a BFO deposition rate of about 1.8 nanometers per minute. After the desired growth time is achieved, the BFO target shutter is closed and the plasma is turned off. A corresponding *in situ* anneal at working temperature with continued sample rotation is done with Ar flow at 0 sccm and O_2 flow at 12 sccm. Anneal times vary for the various sample growths. The chamber heater is then turned off and the sample is cooled to room temperature before removal from the chamber.

Several BFO growth times and *in situ* anneal times were grown throughout the research designed to focus on and study different aspects of the BFO properties. Table 1 represents a list of such samples and will be referenced throughout this thesis by the sample number which corresponds to a date growth (dd/mm/yy).

Table 1. Growth and Anneal Times of BFO on Varied Substrates.

Sample/growth date	Substrate	Estimated thickness	Growth time	Anneal Time[3]
071811	STO//Si	215nm	2 hours	30 minutes
080211	STO//Si	430nm	4 hours	30 minutes
090211	STO//Si	650nm	6 hours	60 minutes
111711	STO//Si	325nm	3 hours	30 minutes
120911	STO//Si	540nm	5 hours	30 minutes
121511	STO//Si	540nm	5 hours	60 minutes
022212[1]	STO//Si	650nm	6 hours	60 minutes
	SiO_2//Si			
062012[1]	STO//Si	650nm	6 hours	60 minutes
	4-1055[2]			
	SiO_2//Si			
082912[1]	STO//Si	650nm	6 hours	60 minutes
	4-1055[2]			
09112	STO//Si	650nm	6 hours	60 minutes
121712	STO//Si	650nm	6 hours	60 minutes

1 - These sputter samples were special growths in which multiple samples were grown at the same time.
2 - This was a special request of epitaxially grown BFO from Dr. Ravi Droopad in the MBE lab at Texas State University. 100A BFO//100A STO//Si(100).
3 - Anneal times were done *in situ.*

CHAPTER 4

RESULTS

This chapter provides the results obtained from various measurement techniques.

X-ray Diffraction

XRD was the initial test of the sputtered BFO to ensure proper growth was achieved in the AJA system. The structure of BFO has been extensively studied and has been found to have a perovskite-type unit cell parameter of 3.965Å and a rhombohedral angle of about 89.3 degrees at room temperature. [14] [5]

Fig. 10 shows the 2θ XRD results of epitaxial BFO sample 4-1055 that was made in Dr. Ravi Droopad's MBE lab. The peaks at about 22, 46, and 72 degrees correspond to the reflection of the (001), (002), and (003) planes respectively when compared to the ICDD and other studies. [15] [16] Sample 4-1055 represents a single crystalline epitaxial growth.

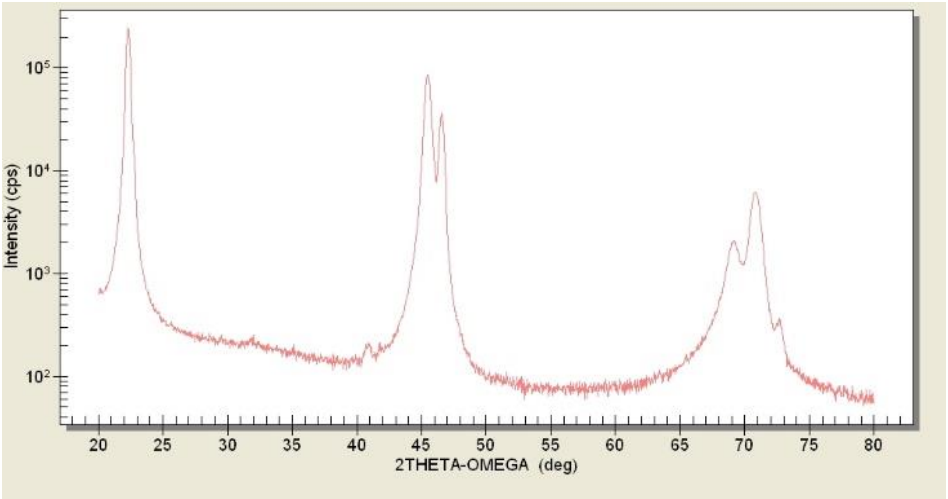

Figure 10. XRD Results of Sample 4-1055.

Fig. 11 shows the 2θ scans of four different BFO samples grown in the AJA. In addition to the peaks of Figure 10, other peaks are observed. The other measured peaks are suspected to represent a polycrystalline growth structure of one or more BFO phases. Fig. 11 shows variant peaks, one at about 32 degrees identified as the (110) plane. The

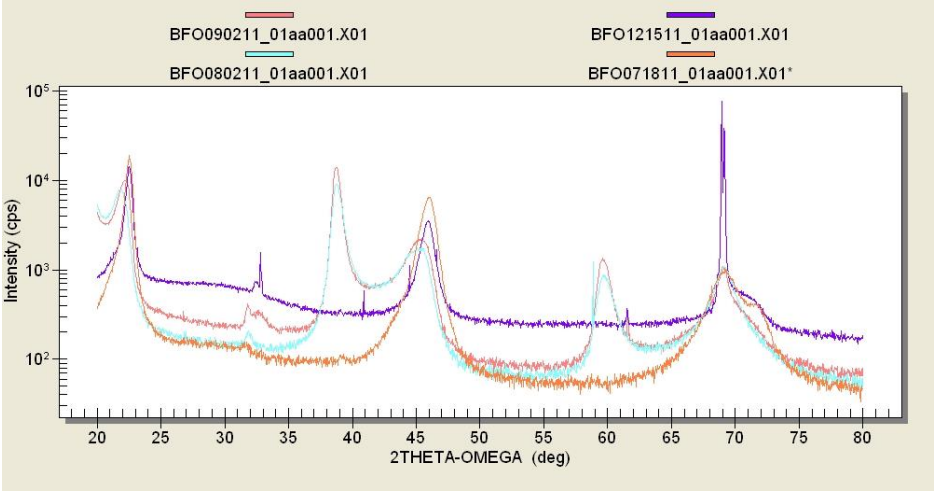

Figure 11. XRD Results of Four BFO Samples. XRD results for BFO samples 071811, 080211, 090211, 121511.

observed peak at 39 degrees represent a (111) plane and the peak at 60 degrees suggests a secondary phase peak of $Bi_2Fe_4O_9$. These results are in agreement with the data found in the ICDD and literature. [17]

The appearance of these secondary BFO phases or textures become more prominent as the BFO film thickness is increased. Samples 071811 and 121511 show strong indications of single crystalline growth. These two sample are on opposite ends of our thin film thicknesses. This gives confidence in being able to further optimize growth procedures to consistently reproduce single crystalline thin films. It is unclear whether the observed surface structures (discussed later in this chapter) have a direct influence on the XRD results.

Vibrating Sample Magnetometer

Various VSM results are recorded as a raw data file and imported into Excel as a delimited file for viewing. This data file provided recorded information from the PPMS including but not limited to: temperature, magnetic field, moment, time, frequency, amplitude, position, individual coil signals, several averaging errors, etc. Our interest was with the magnetic field and moment. These two columns of information are used to assemble a hysteresis curve.

Each sample was run through two different scans, a high magnetic field scan and a low magnetic field scan. A typical high magnetic field scan is shown in Fig. 12. The negative slope at high magnetic fields is caused by the diamagnetic properties from the sample, sample holder, and substrate material. Diamagnetism, the property of a material to have a magnetization that is proportional but opposite of an applied external field, is clearly present in our sample. These high magnetic field scans are done to obtain the diamagnetic slope so the previously described diamagnetic contribution may be removed in the following low magnetic field scans to better observe the hysteresis. The

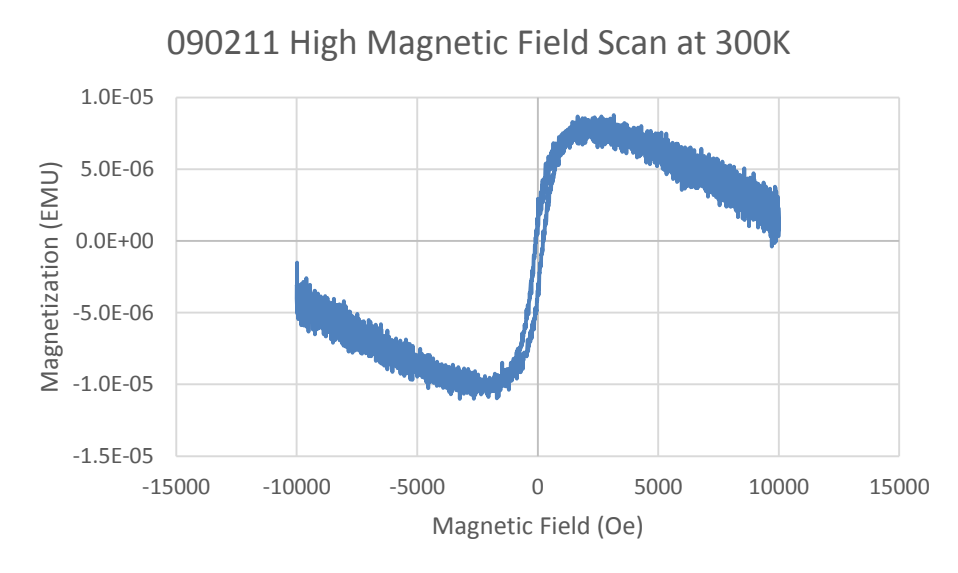

Figure 12. 090211 High Magnetic Field Scan at 300K.

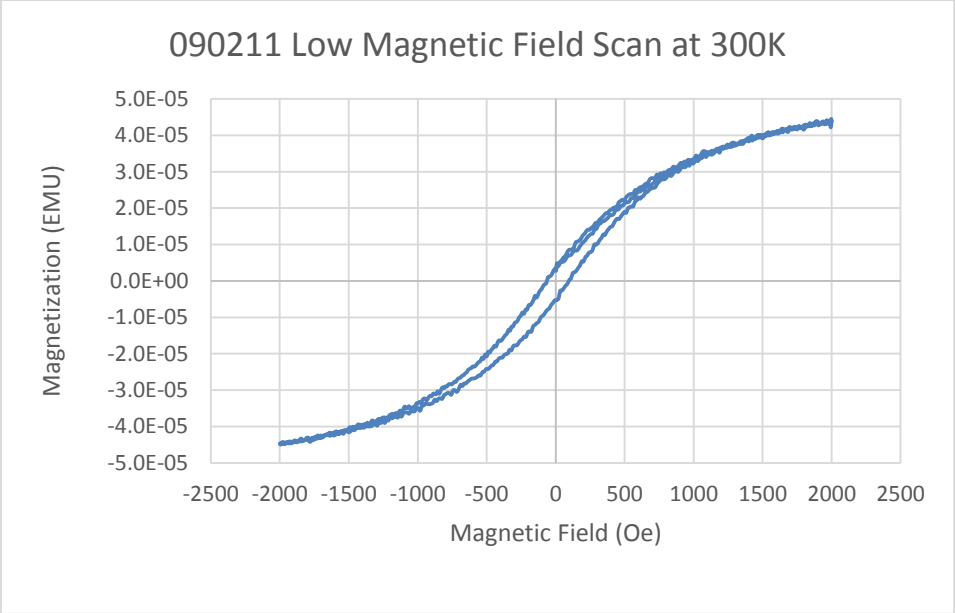

Figure 13. 090211 Low Magnetic Field Scan at 300K

diamagnetic slope of the high magnetic field scan is calculated using Excel on each side of the graph and averaged. Then a low magnetic field scan is measured, as for example sample 09011 scan shown in Fig. 13. This approach allow us to focus in on the hysteresis area of the hysteresis curve and to more accurately observe coercivity and remanence values. The hysteresis curve is then adjusted using the diamagnetic slope previously obtained from the high magnetic field scan. The curve is adjusted by the following equation:

Adjusted magnetic moment = original magnetic moment - (diamagnetic slope * original magnetic field)

This equation is applied to the moment data set to create a new column in Excel. This new column is graphed with the original magnetic field to produce the adjusted hysteresis curve. This removes any diamagnetic influence from the desired BFO magnetism results. Fig. 14 shows the VSM scan of sample 090211 with the adjusted results and the original results overlaid. Fig. 15 shows an alternative representation of VSM data from sample 090211. This provides the remanent magnetization and

coercivity values. This shows a slight change in saturation value confirming a small diamagnetic influence in the smaller magnetic fields.

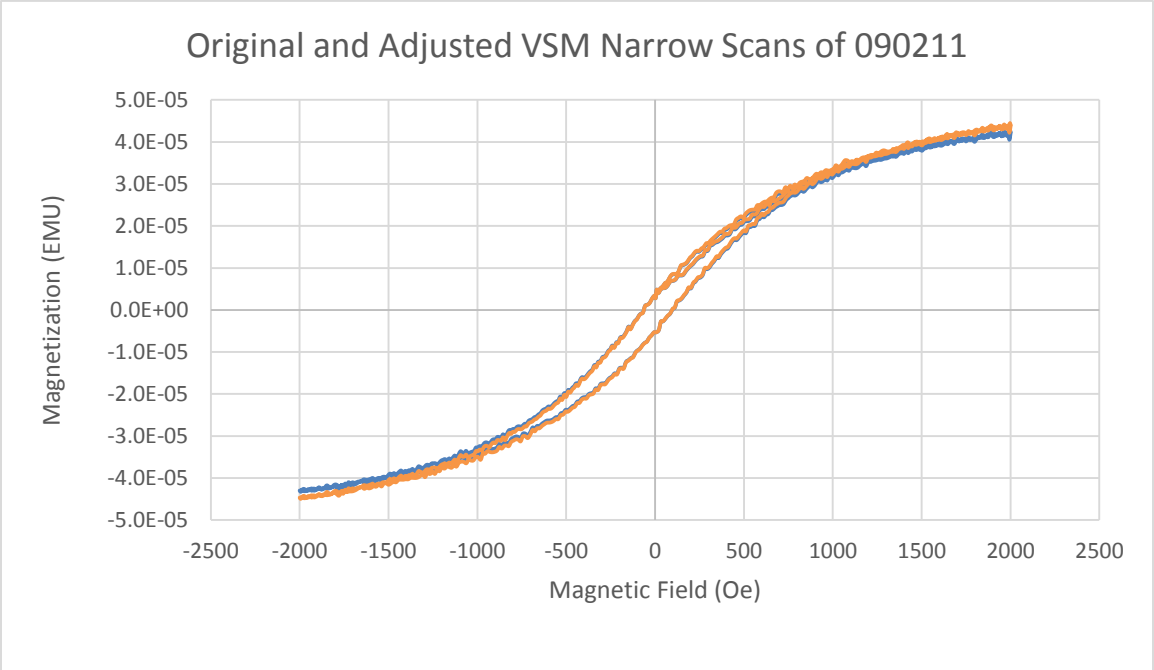

Figure 14. Original and Adjusted Low Magnetic Field Scans of Sample 090211.

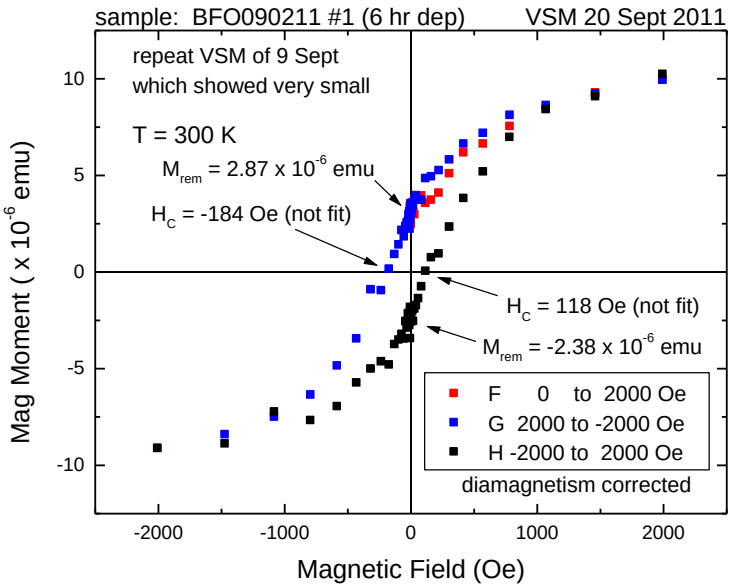

Figure 15. Alternate Low Magnetic Field Scan of Sample 090211.

This correction is not an ideal method for diamagnetic adjustment. This method was used as no magnetic fingerprint was measured for the sample holder or substrates. The previously described method and correction assumed our high magnetic field scans were high enough to achieve complete saturation to veiw the diamagnetism.

BFO sample 090211 was also put through a series of temperature dependent VSM scans. This provided information on the magnetization property under different conditions. 090211 had a low field scan at 4.2, 50, 100, 150, 200, 250, and 300K. A high field scan was also done at 4.2K and 300K to provide a diamagnetic slope at both extremes of out temperature test. A linear curve was applied to these slopes to extrapolate additional diamagnetic slope values for the intermediate scans. Fig. 16 shows the temperature dependent scans of sample 090211.

The small changes measured in the temperature dependent scans indicate we are near the PPMS's measurement capabilities. No trend could be extract from this measurement. This could also verify the Neel temperature ($T_N \sim 643K$) [5] of BFO confirming a steady state at low through room temperature. This weak BFO ferromagnetic thin film measurement at low magnetic fields, permitted by the R3*c* [18] space group, is verified by other studies [5] [19] as compared to the measured antiferromagnetic properties of bulk BFO. [14]

These temperature dependent scans unfortunately have varied magnetic field parameters throughout. This skews the visible and measureable components of the hysteresis making it difficult to accurately compare results. This measurement should be re-done with identical parameters for each variant temperature.

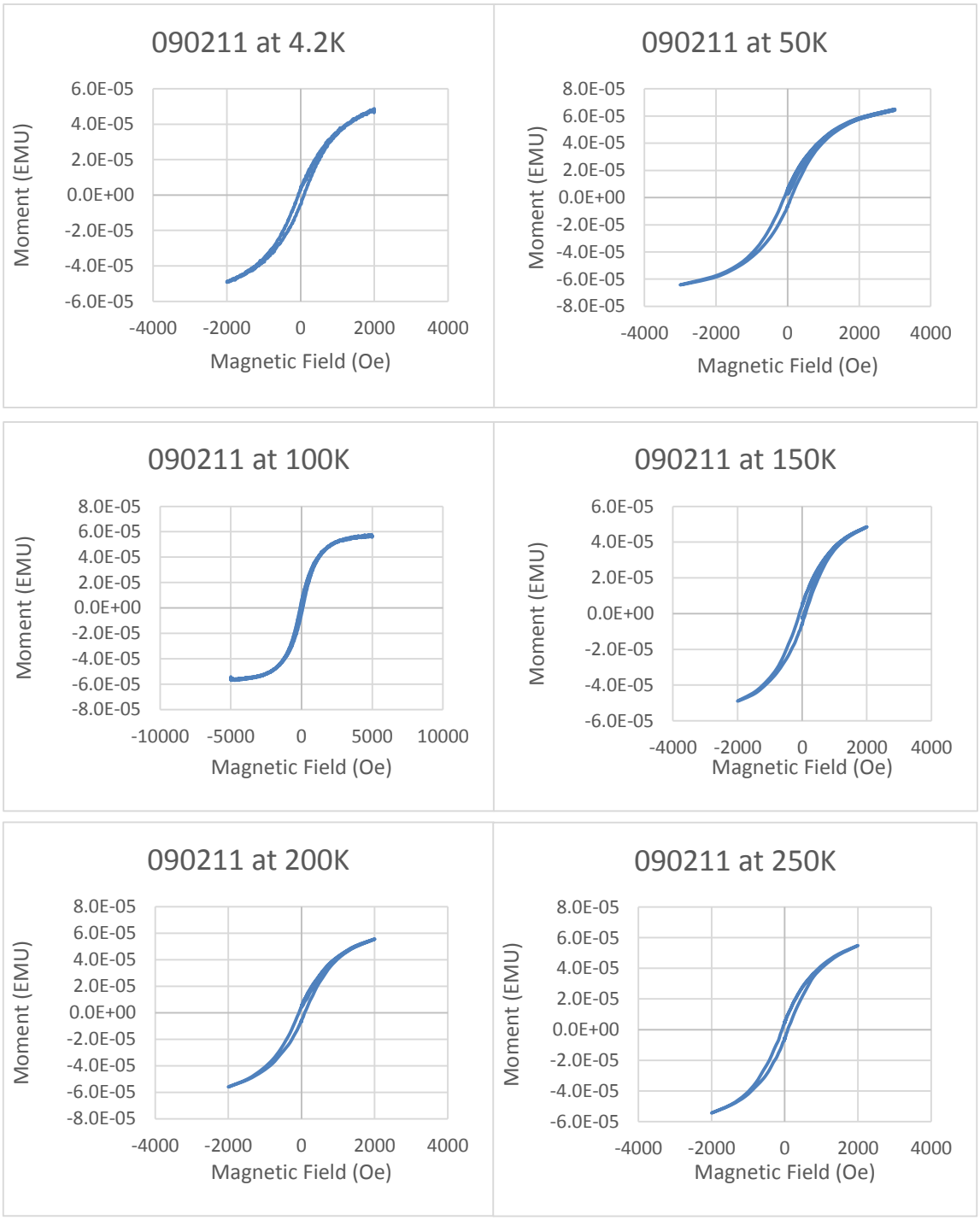

Figure 16. VSM Results of Sample 090211 at Various Temperatures.

Scanning Electron Microscope

Scanning Electron Microscopy was used to characterize the surface morphology of the sample. Any observation in the surface growth structure could help lead to understanding of BFO growth during RF magnetron sputtering. Observation of the earlier shorter sputter times revealed that the post-deposition surface was fairly uniform

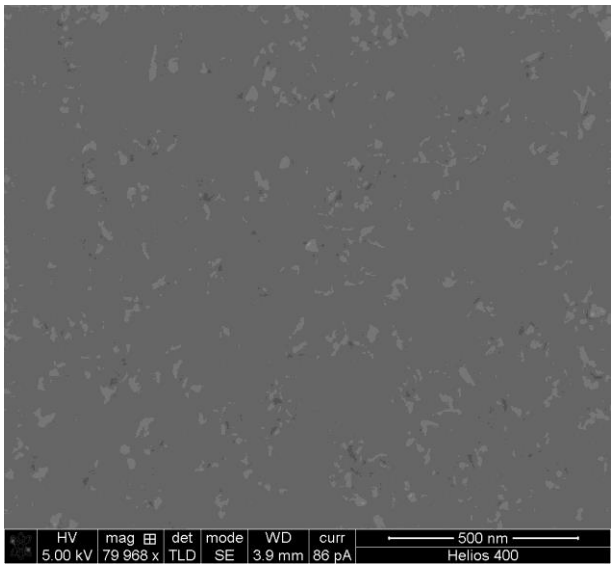

Figure17. SEM Surface Image of Sample 070811

with a tiled like surface as shown in Fig. 17. These results were comparable to the surface morphologies seen in previous studies.[20, 21, 22] Inspection of the longer BFO depositions also revealed similar surface results as shown in Fig. 18. Further SEM

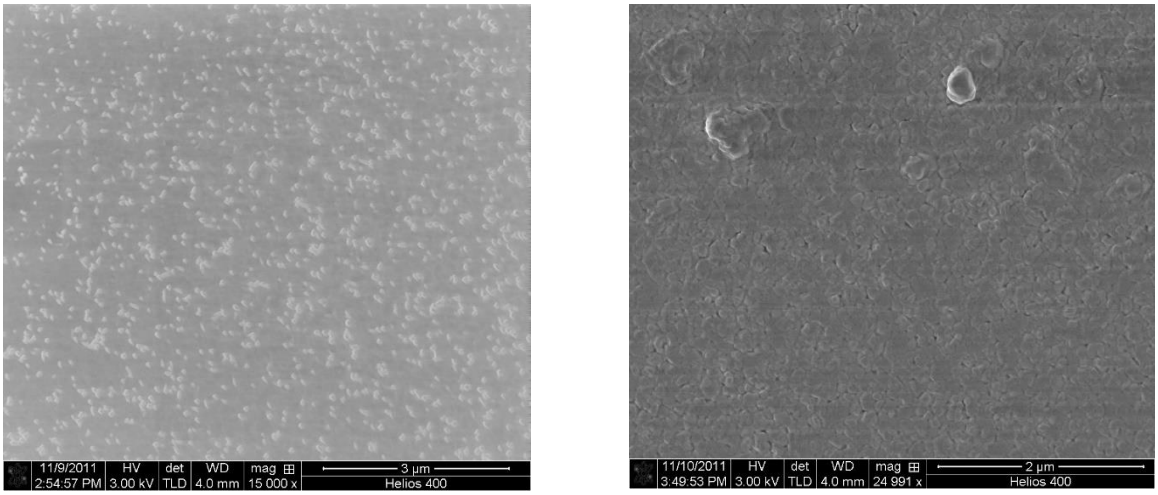

Figure 18. SEM surface images of sample 111711 (Left) and 080211 (Right).

surface imaging on the thicker BFO films resulted in the discovery of circular structures in what appeared to be on mostly the entire surface of the samples. As shown in Fig. 19, an array of circular structures can be seen on sample 090211. These images show similar size circles (about 6 μm) and comparable spatial distances organized in a hexagonal type

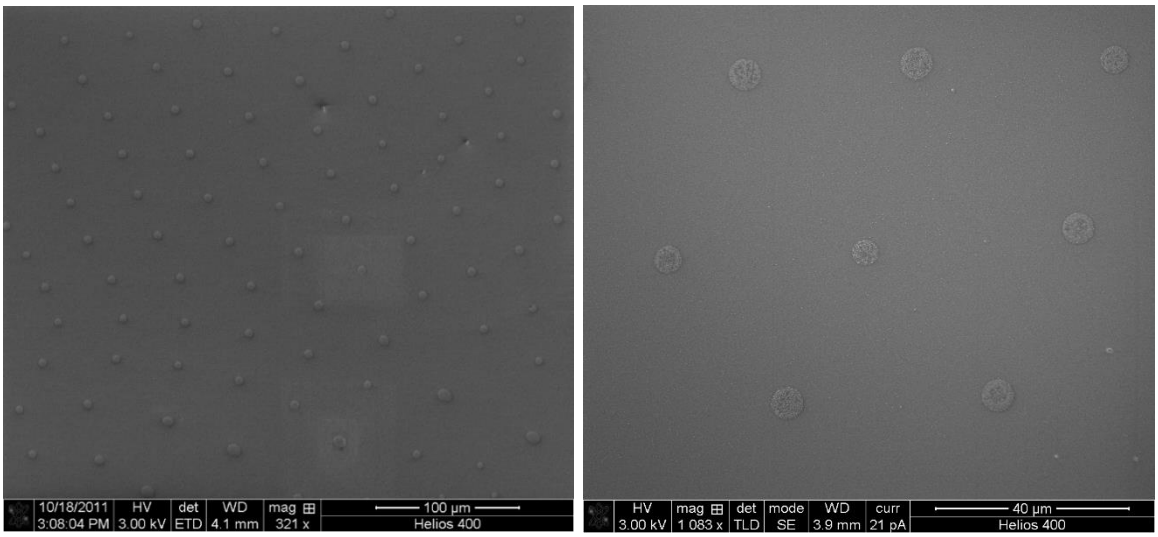

Figure 19. SEM Surface Images of Sample 090211. Array of self-assembled circular structures on surface of sample 090211.

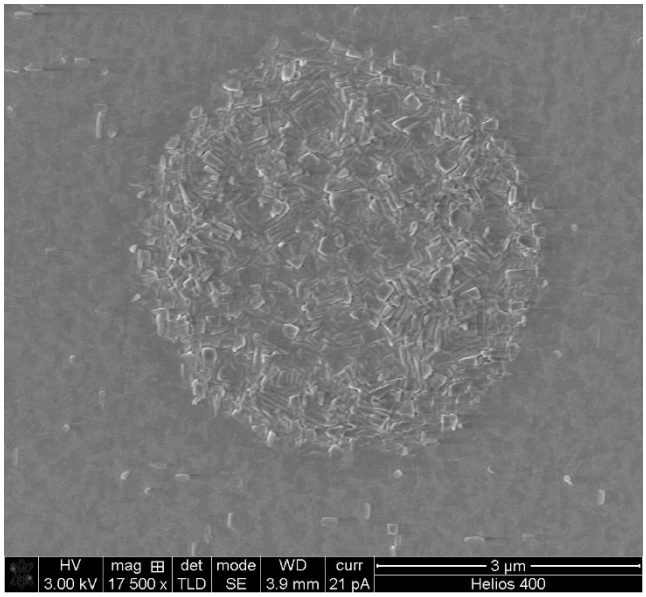

Figure 20. SEM Close-up Image of Circular Structure on Sample 022212.

arrangement. The area between circular structures revealed a tiled surface similar to those already seen on previous samples. Fig. 20 shows a close up image of a circular

structure with the typically seen tiled surface surrounding it. This image also shows a much higher concentration of tiled structures in the interior area of the circle. These images represent the typically seen structure of the observed formations across the sample surfaces. The focus of the research was then altered to the understanding of these formations.

At the time of the discovery of these structures on sample 090211 (also known as growth date 09/02/2011), only 2, 4, and 6 hour depositions were grown. Further depositions were done in order to view the growth evolution of these circular structures. Table 1 in chapter 3 shows the addition of a 3 and 5 hour deposition with varying anneal times on the 5 hour samples. A unique image was discovered upon further examination of the surface structure. As shown in Fig 21, the cleaved edge of sample 090211 provided a cross sectional view of one of the structures. As another comparison, BFO was grown on bare SiO_2 for sample 022212. Figure 22 shows an SEM image of the BFO

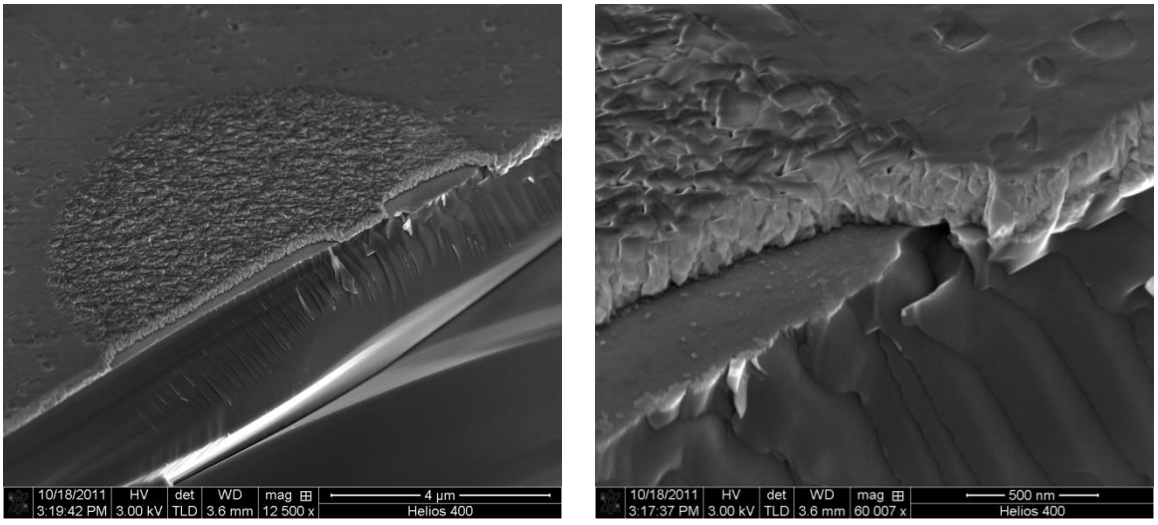

Figure 21. SEM Close-up Images of Cut Away Circular Structure on Sample 090211

surface again showing the circle structures. Instead of the ordered array and equal distance spacing between circles, it can be seen that these circles appear to be randomly distributed although the size of these circles are comparable in diameter to the other

deposition samples. This does however imply that these circles are affected or influenced by the substrate material. The preferred orientation of the observed BFO surface

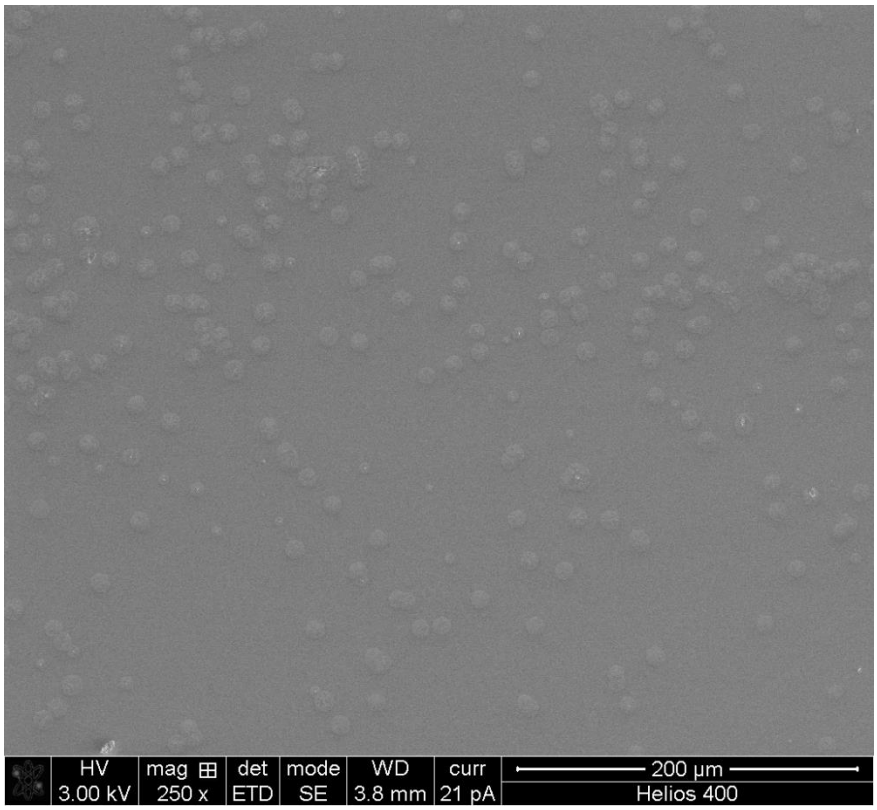

Figure 22. SEM Surface Image of 022212 on SiO_2.

structures correspond with either the amorphous SiO_2 or the epitaxial STO substrates. Still unsure of the circular structure's development, further growths were done.

To determine whether the circular defects were due to substrate preparation, BFO was grown simultaneously on three different substrates (SiO_2, STO, and sample 4-1055) for sample 062012. The findings of these samples returned negative results. No sign of any circular structures appeared on any sample. Three more growths were done to try and reproduce previously seen circular structures with samples 082912, 91112, and 121712. These also returned negative results on desired substrates. But surprisingly, circular structures were found on the 4 inch silicon pilot wafer used on sample holder inside the growth chamber. This deposition used a new pilot wafer for the growth and

found identical surface structures as compared to the 022212 growth on SiO_2. To further investigate these circular structures, use of the SEM's energy-dispersive x-ray spectroscopy, also known as EDX, capabilities were used.

Energy Dispersive X-ray Spectroscopy

EDX can provide insight in to any growth changes throughout the sputtering process. This technique allowed us to look for any compositional changes, impurities, or contaminations in any of the samples that could provide insight into the formation of circular structures or the disappearance of them.

Further growth verification of BFO was also done with EDX. The EDX software allows for the option to choose and measure designated elements. To verify desired BFO growth by the AJA, only the elements Bi, Fe, and O were selected for detection and the results show a consistent composition of about 15:20:65 respectively was recorded as shown in table 2 of sample 022212. This verified a growth of the desired $BiFeO_3$ composition of 20:20:60.

Table 2. eZAF Smart Quant Results.

Element	Weight %	Atomic %	Net Int.	Net Int. Error
O K	19.59	65.37	249.43	0.01
Bi M	60.31	15.41	864.58	0
Fe K	20.1	19.22	166.61	0.02

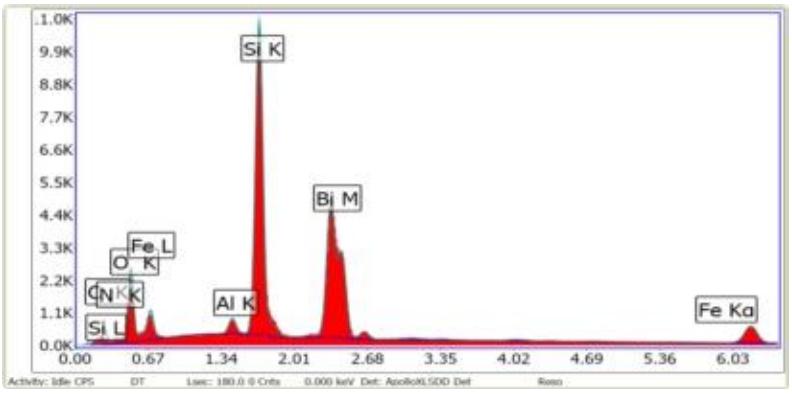

Figure 23. EDX Results of Sample 091112.

The EDX results provided an insight into any change in growth composition throughout research. Several samples were analyzed and found a curious spike of aluminum traces in a number of samples. Fig. 23 shows a clear aluminum peak on sample 091112 which does not contain any surface circular structures. Sample 022212, which does contain circular structures, was scanned and resulted in an aluminum peak as well. This information suggests that the supposed aluminum contamination does not have an effect on the origin of the observed circular structures.

The AJA does share lab time with other professors and students for different studies. These other growths have been thoroughly tracked within the AJA log book and we found previous aluminum depositions within the chamber previous to our BFO growths. This led us believe the aluminum contamination originated in the growth chamber of the AJA. This then led to a much needed cleaning of the main growth chamber on 12/5/2012. All RF and DC magnetron guns were removed and cleaned with an 80 grit alumina media recommended by the AJA manufacturer. Other equipment media blasted included sample holder, target holders, target chimneys, and target shutters. The interior of the chamber was then wiped with isopropyl alcohol. All blasted parts were also cleaned with IPA in a sonic cleaning bath. All parts were dried and reassembled and the chamber was then pumped down over night to working pressure. A final BFO sample was grown to check for further contamination and any growth changes. Sample 121712 had an identical growth procedure to the previous 6 hour samples and was also found to contain no structures. When scanned by the EDX, results were comparable in composition to previous sample with no observed aluminum peak. However, after the chamber cleaning, a new silicon pilot wafer was placed on the sample

holder for growth. Out of curiosity, this wafer was imaged and was found to contain circular structures similar to those found previously on silicon substrates. They were found to be similar in size and random ordering as previously found on sample 022212. This provided even more confusion to the origin of circular structures.

To further investigate the origin of the believed aluminum contamination, a final EDX scan of samples 071811, 080211, 090211, 022212, 091112, 4-1055, and a silicon test sample were done to catalog any measurable changes in composition. All of these results showed no sign of aluminum including the previously scanned samples. This suggests previous sample scans may have measured a series of backscattered or secondary electrons resulting in false readings. These secondary electrons can be emitted from the BFO surface with enough energy to hit a chamber wall or piece of internal equipment and eject another electron to be detected by the EDX. These results did however provide us with a chronology of BFO growth composition. All EDX results can be found in Appendix A.

Atomic Force Microscope

Further investigation into the topographical structures lead us to view AFM images in hope of further understanding the formation of the circles. Fig. 24 shows an AFM scan of sample 090211 with a circular structure centered in the 15μm scan. This image verifies previously seen structures observed on the SEM. A textured surface with

a high density of tiled structures within the circular structure's interior surface area are verified with the AFM.

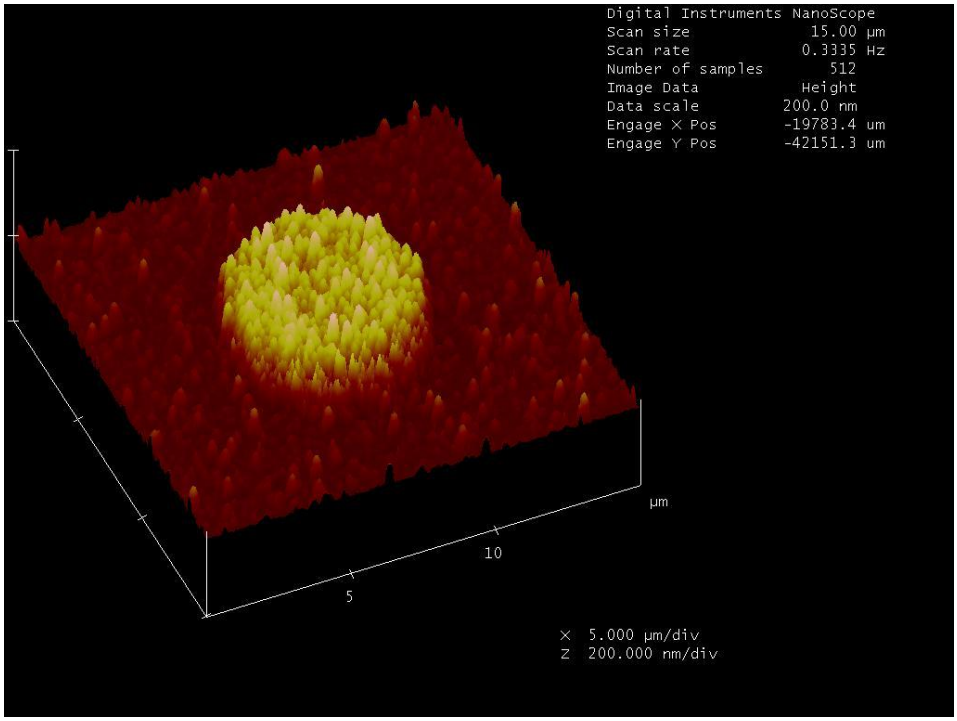

Figure 24. AFM Image of Sample 090211.

CHAPTER 5

CONCLUSION

The purpose of this thesis was to establish a consistent growth technique for $BiFeO_3$. As previously described, BFO is a material that is highly applicable and practical due to its ability to display simultaneous properties of antiferromagnetic and ferroelectric properties at room temperature. This material is still highly popular in research and its properties are still being investigated. This research will provide a solid background of growth techniques for further research projects.

This project provides a unique opportunity at Texas State University-San Marcos in that the epitaxial $SrTiO_3$/Si substrate is grown here on campus in the molecular beam epitaxy lab under the supervision of Dr. Ravi Droopad. This provides an opportunity to adjust substrate parameters at an efficient cost and time. The BFO film can then be optimized for research application needs.

This research has found an acceptable formula for depositing BFO on epitaxially grown STO in the ATC ORION 5 UHV RF magnetron sputtering system at 600°C. XRD results show the resulting films to be consistently polycrystalline within a range of thickness from 200nm – 600nm. Desired growth composition was confirmed using the scanning electron microscope's EDX system. EDX scans revealed consistent film composition of the desired $BiFeO_3$ elements.

The unexpected discovery of the observed surface features took the characterization goals in a new direction. These structures were investigated using the SEM and AFM. Variation in growth time, anneal time, and substrate material were varied to study the structures origins. Our investigatory growths were then halted by the unknown cause of not being able to reproduce the circular structures.

These findings provide an interesting avenue of study for the formation of these structures as no papers were found that discuss this phenomenon. The next step I would like to see in the exploratory studies on these circular structures would be TEM imaging with instrumentation acquired in the future or obtained through a neighboring university. I believe these images could provide insight into the formation of the structures and its dependence on the STO interface if any.

If these circular structures prove to be non-reproducible or in fact a very common artifact, there is still a lot of research to be done on the BFO thin film itself. Work still need to be done on characterizing the crystal structure observed during our unique growth process. More sensitive VSM studies also need to be done to help characterize the magnetic properties of BFO. Then there is of course the eventual studies of device applications available for this material. There is still a lot of work to be done on this research and a lot of prospective research opportunities available for this project and for this university.

APPENDIX A

EDX RESULTS

Initial EDX scan of sample 090211 with suspected aluminum peak.

EDAX TEAM EDS

Rye-BFO

Author: supervisor
Creation: 9/17/2012
Sample Name: BFO

Area 22

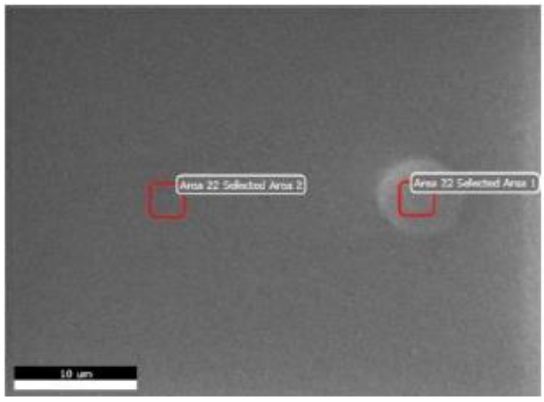

Notes:

Selected Area 1

Det 1 kV: 15 Mag:6497 Takeoff:28.9 Live Time:180 Amp Time:12.8 Resolution:129.8

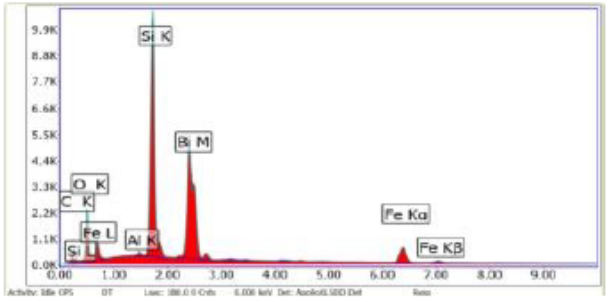

Element	Weight %	Atomic	Net Int.	Net Int. Error
C K	7.73	23.09	16.53	0.03
O K	14.69	32.93	75.55	0.01
Al K	0.07	0.1	1.37	0.6
Si K	23.36	29.84	474.01	0
Bi M	44.07	7.57	251.78	0.01
Fe K	10.08	6.47	48.93	0.03

EDAX TEAM EDS

Selected Area 2

Det 1 kV: 15 Mag:6497 Takeoff:28.9 Live Time:180 Amp Time:12.8 Resolution:129.8

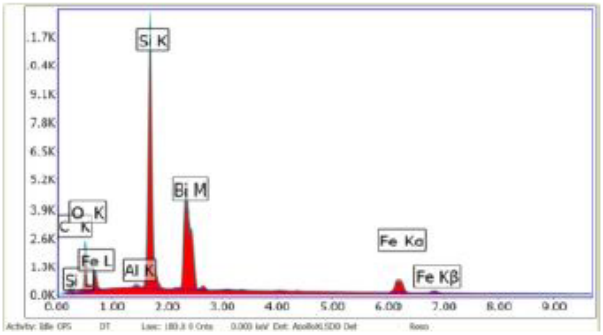

Element	Weight %	Atomic	Net Int.	Net Int. Error
C K	8.11	22.8	16.14	0.03
O K	15.01	31.68	79.98	0.01
AlK	0.14	0.18	2.82	0.44
SiK	27.34	32.87	576.02	0
BiM	39.27	6.34	227.25	0.01
FeK	10.11	6.11	50.06	0.03

Follow up EDX scan of sample 022212 to confirm suspected aluminum peak.

EDAX TEAM EDS Page1

Rye-BFO

Author: supervisor
Creation: 9/17/2012
Sample Name: BFO

Area 21

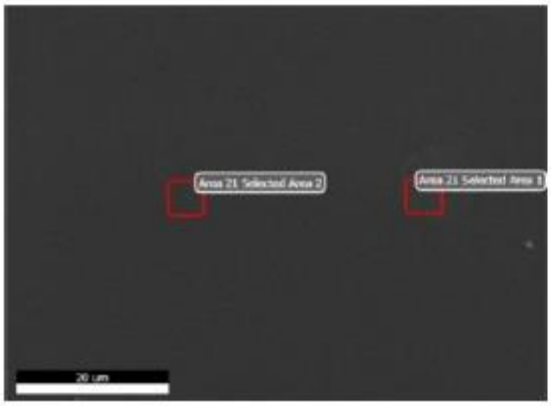

Notes:

Selected Area 1

Det 1 kV: 15 Mag:4000 Takeoff:29 Live Time:180 Amp Time:12.8 Resolution:129.8

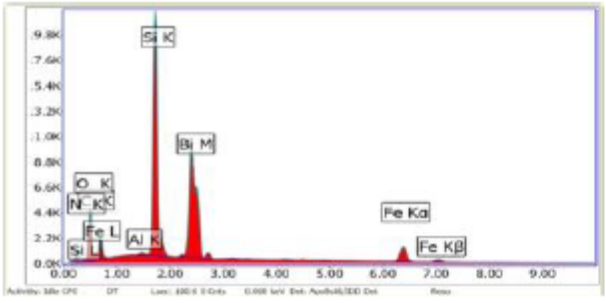

Element	Weight %	Atomic	Net Int.	Net Int. Error
C K	6.75	19.52	29.73	0.02
N K	2.33	5.78	9.02	0.06
O K	14.85	32.25	154.97	0.01
Al K	0.15	0.2	5.89	0.22
Si K	23.28	28.79	975.27	0
Bi M	42.27	7.03	496.8	0.01
Fe K	10.37	6.45	103.7	0.02

EDAX TEAM EDS

Page2

Selected Area 2

Det 1 kV: 15 Mag:4000 Takeoff:29 Live Time:180 Amp Time:12.8 Resolution:129.8

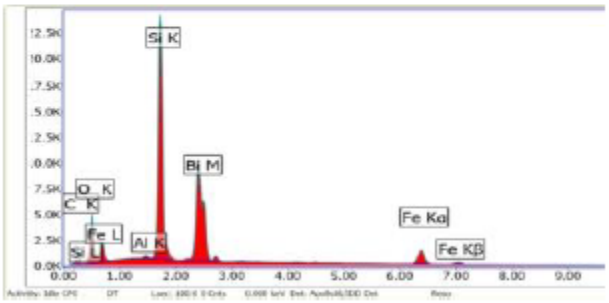

Element	Weight %	Atomic	Net Int.	Net Int. Error
C K	7.71	22.08	31.21	0.02
O K	15.1	32.48	160.57	0.01
AlK	0.18	0.23	6.79	0.18
SiK	26.15	32.04	1088.28	0
BiM	40.24	6.63	464.14	0.01
FeK	10.62	6.55	104.65	0.02

The previous results of initial EDX scans of sample 090211 and 022212 verified our suspected theory of growth contamination in the AJA main chamber. This lead to the pump down and cleaning of the main chamber and AJA sputtering system components.

The following EDX scans provided us with a general catalog of the BFO growth composition. These scans were done one after the other to preserve identical conditions in the SEM chamber. The first EDX scan was a piece of bare silicon to provide a background reading.

EDAX TEAM

Page 1

Rye-BFO

Author: supervisor
Creation: 3/31/2013
Sample Name: BFO

Area 27

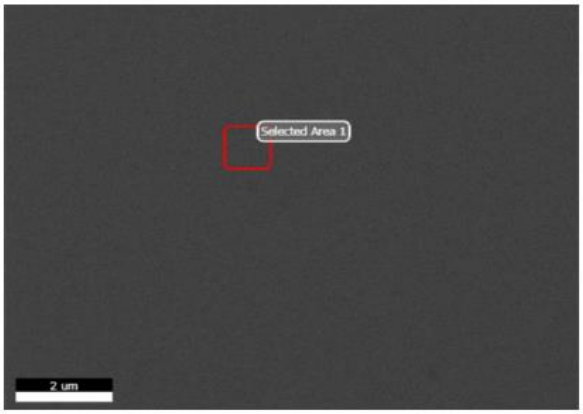

Notes:

EDAX TEAM

Selected Area 1

kV: 15 Mag: 24000 Takeoff: 29 Live Time(s): 100 Amp Time(µs): 12 Resolution:(eV)130.2

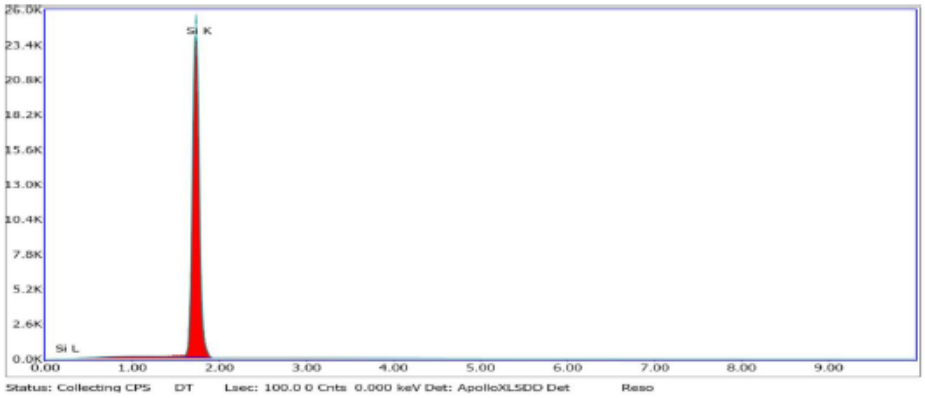

eZAF Smart Quant Results

Element	Weight %	Atomic %	Net Int.	Net Int. Error
SiK	100	100	2144.96	0

EDX scan of sample 071811

EDAX TEAM

Page 1

Rye-BFO

Author: supervisor
Creation: 3/31/2013
Sample Name: BFO

Area 28

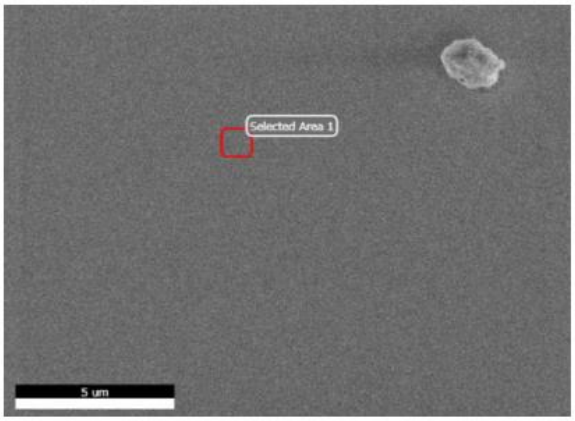

Notes:

EDAX TEAM

Selected Area 1

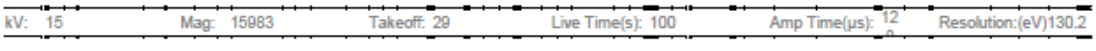

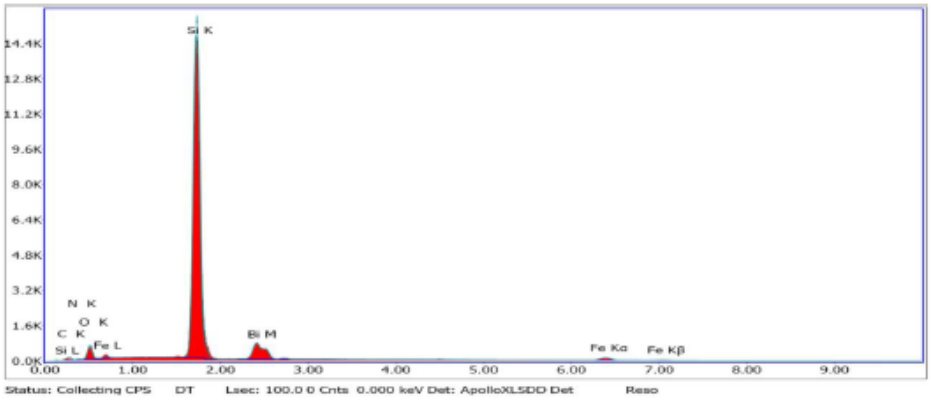

eZAF Smart Quant Results

Element	Weight %	Atomic %	Net Int.	Net Int. Error
C K	5.01	11.74	4.43	0.09
N K	1.27	2.55	1.58	0.26
O K	8.78	15.43	39.02	0.02
SiK	65.79	65.91	1304.3	0
BiM	14.34	1.93	68.29	0.04
FeK	4.81	2.42	15.12	0.11

eZAF Smart Quant Results

Element	Weight %	Atomic %	Net Int.	Net Int. Error
O K	29.89	76.49	43.6	0.02
BiM	51.9	10.17	76.64	0.01
FeK	18.2	13.34	15.26	0.11

EDX scan of sample 080211.

EDAX TEAM

Rye-BFO

Author: supervisor
Creation: 3/31/2013

Sample Name: BFO

Area 30

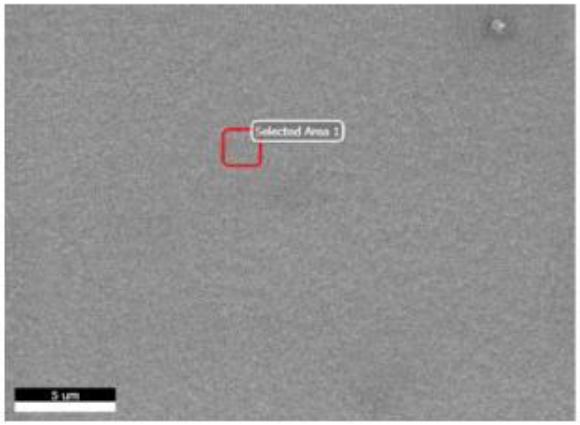

EDAX TEAM

Selected Area 1

kV: 15 Mag: 10000 Takeoff: 28.9 Live Time(s): 100 Amp Time(µs): 12 Resolution:(eV)130.2

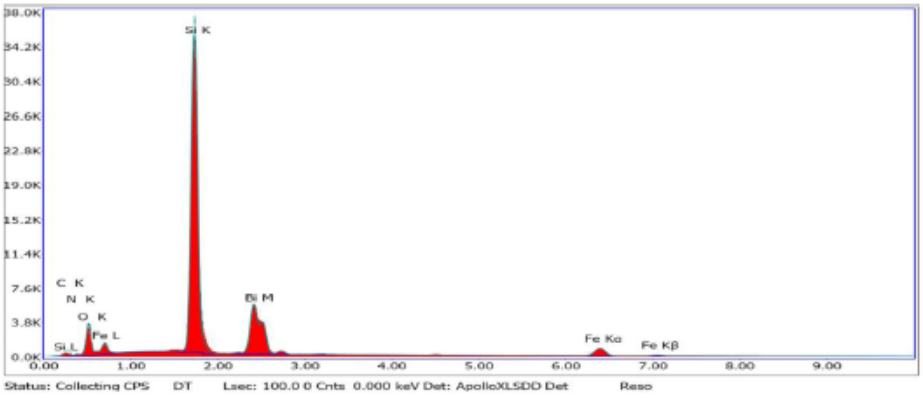

eZAF Smart Quant Results

Element	Weight %	Atomic %	Net Int.	Net Int. Error
C K	4.83	12.58	22.56	0.04
N K	2.05	4.57	11.56	0.07
O K	12.35	24.13	216.02	0.01
SiK	44.39	49.41	3110.4	0
BiM	26.93	4.03	519.65	0.01
FeK	9.45	5.29	114.66	0.02

eZAF Smart Quant Results

Element	Weight %	Atomic %	Net Int.	Net Int. Error
O K	24.18	70.86	220.12	0.01
BiM	56.09	12.58	546.39	0
FeK	19.73	16.56	110.16	0.02

EDX scan of sample 090211.

EDAX TEAM

Rye-BFO

Author: supervisor
Creation: 3/31/2013
Sample Name: BFO

Area 31

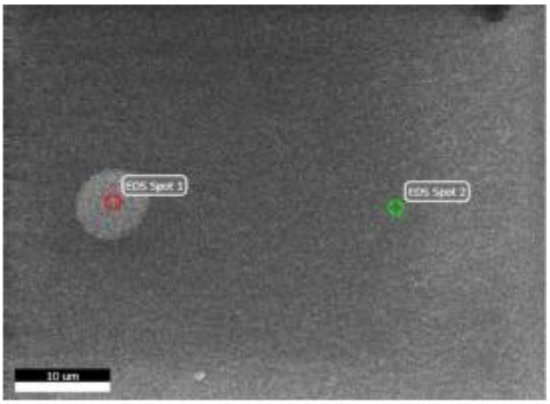

Notes:

EDAX TEAM

EDS Spot 1

kV: 15 Mag: 5000 Takeoff: 29 Live Time(s): 100 Amp Time(µs): 12 Resolution:(eV)130.2

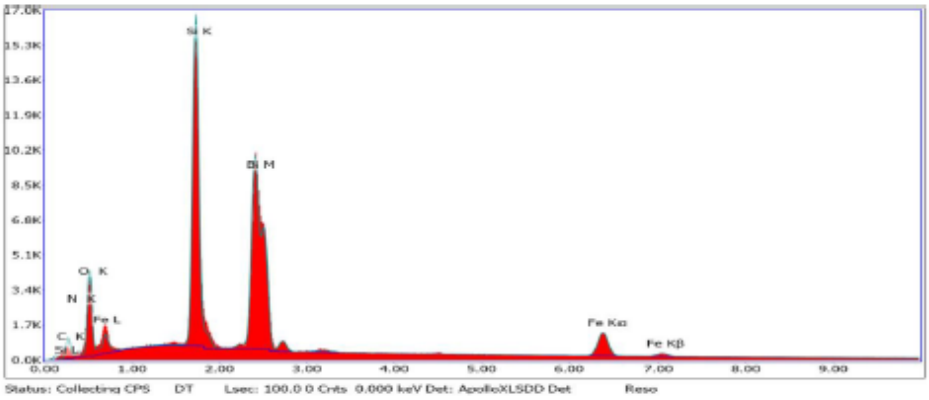

eZAF Smart Quant Results

Element	Weight %	Atomic %	Net Int.	Net Int. Error
C K	4.39	13.85	31.85	0.03
N K	2.05	5.54	13.49	0.07
O K	14.66	34.69	253.05	0.01
SiK	21.41	28.86	1351.79	0
BiM	44.1	7.99	887.75	0.01
FeK	13.39	9.08	161.7	0.02

EDAX TEAM

EDS Spot 2

kV: 15 Mag: 5000 Takeoff: 29 Live Time(s): 100 Amp Time(µs): 12 Resolution:(eV)130.2

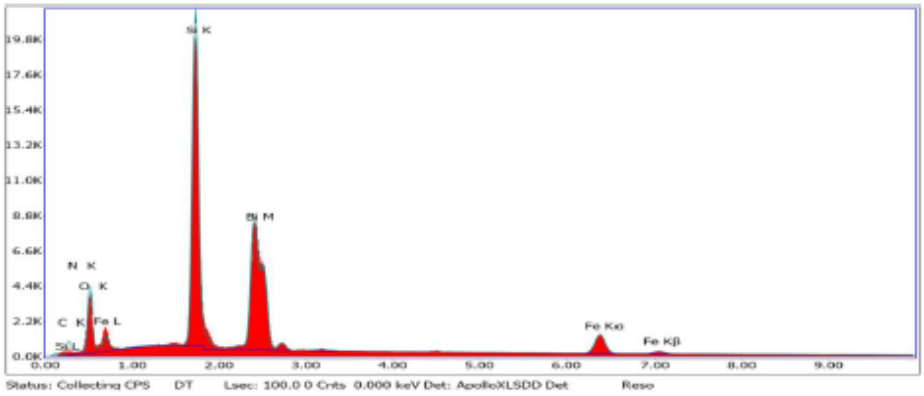

eZAF Smart Quant Results

Element	Weight %	Atomic %	Net Int.	Net Int. Error
C K	4.28	12.76	27.77	0.03
N K	2.07	5.29	13.47	0.07
O K	14.41	32.27	257.05	0.01
SiK	26.92	34.34	1765.6	0
BiM	38.78	6.65	784.78	0.01
FeK	13.54	8.69	166.21	0.02

EDX scan of sample 022212 sputtered on STO.

EDAX TEAM

Page1

Rye-BFO

Author: supervisor
Creation: 3/31/2013
Sample Name: BFO

Area 32

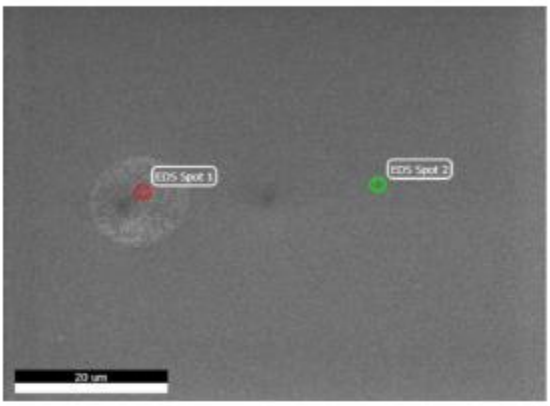

Notes:

EDAX TEAM

EDS Spot 1

kV: 15 Mag: 4000 Takeoff: 29 Live Time(s): 100 Amp Time(µs): 12 Resolution:(eV)130.2

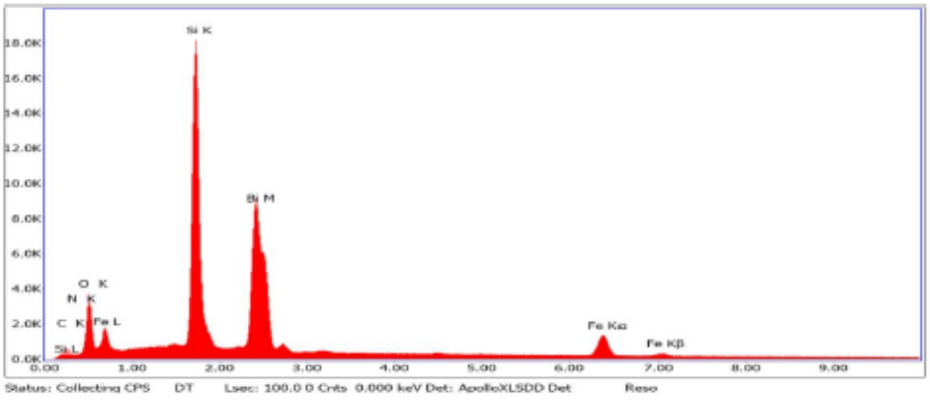

eZAF Smart Quant Results

Element	Weight %	Atomic %	Net Int.	Net Int. Error
C K	4.21	12.98	28.3	0.03
N K	2.02	5.34	13.16	0.07
O K	13.93	32.26	245	0.01
SiK	24.93	32.89	1607.75	0
BiM	40.92	7.25	825.12	0.01
FeK	13.99	9.28	170.53	0.02

eZAF Smart Quant Results

Element	Weight %	Atomic %	Net Int.	Net Int. Error
O K	19.59	65.37	249.43	0.01
BiM	60.31	15.41	864.58	0
FeK	20.1	19.22	166.61	0.02

EDAX TEAM

EDS Spot 2

kV: 15	Mag: 4000	Takeoff: 29	Live Time(s): 100	Amp Time(µs): 12	Resolution:(eV)130.2

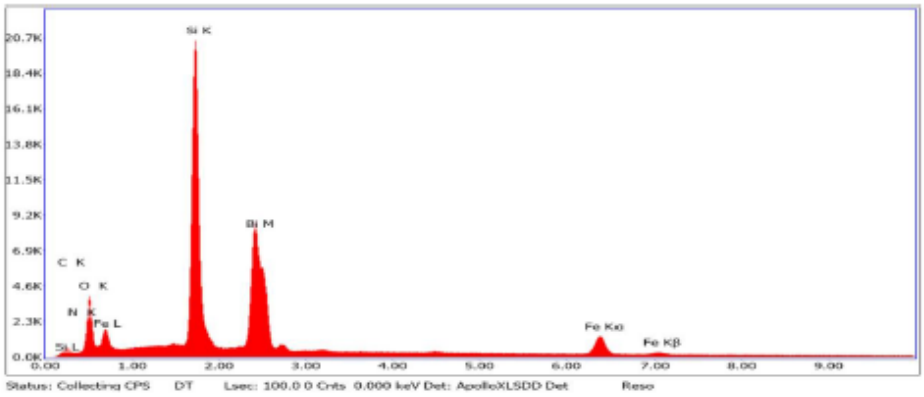

eZAF Smart Quant Results

Element	Weight %	Atomic %	Net Int.	Net Int. Error
C K	4.38	12.91	28.35	0.03
N K	2.17	5.5	14.24	0.06
O K	14.36	31.81	259.16	0.01
SiK	27.37	34.53	1813.93	0
BiM	37.78	6.41	771.23	0.01
FeK	13.94	8.84	172.59	0.02

eZAF Smart Quant Results

Element	Weight %	Atomic %	Net Int.	Net Int. Error
O K	20.89	66.64	264.79	0.01
BiM	58.16	14.21	811.24	0
FeK	20.95	19.15	168.49	0.02

EDX scan of sample 4-1055 epitaxially grown in the MBE lab supervised by Dr. Ravi Droopad.

EDAX TEAM *Page 1*

Rye-BFO

Author: supervisor
Creation: 3/31/2013
Sample Name: BFO

Area 33

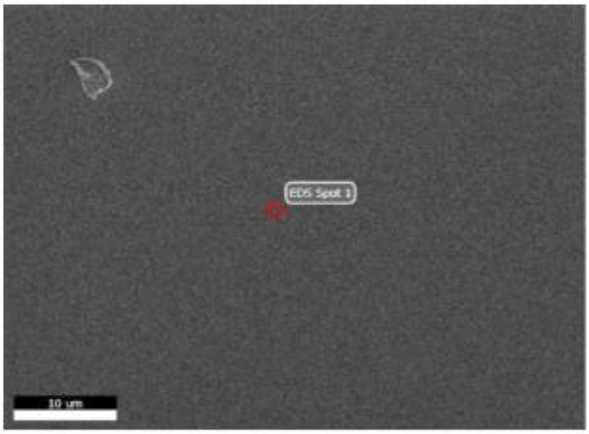

Notes:

EDAX TEAM

EDS Spot 1

kV: 15 Mag: 5000 Takeoff: 29 Live Time(s): 100 Amp Time(μs): 12.8 Resolution:(eV)130.2

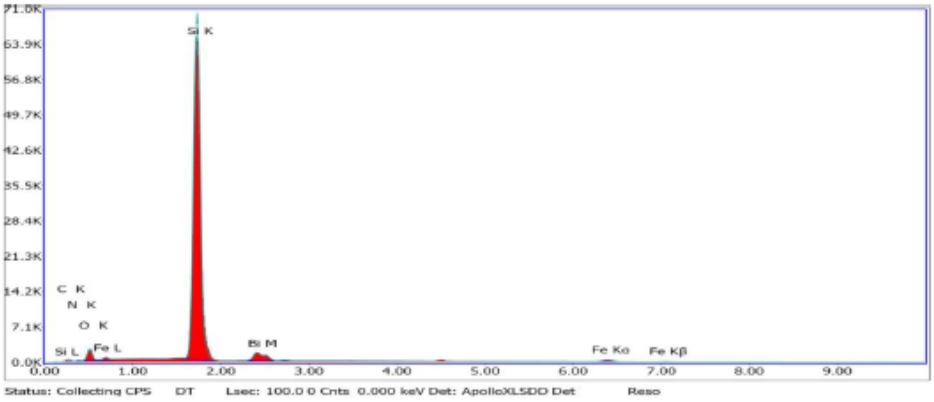

eZAF Smart Quant Results

Element	Weight %	Atomic %	Net Int.	Net Int. Error
C K	4.96	10.93	15.59	0.05
N K	1.78	3.37	8.3	0.09
O K	8.63	14.29	149.23	0.01
SiK	72.95	68.78	5853.54	0
BiM	8.35	1.06	153.42	0.03
FeK	3.33	1.58	40.92	0.06

eZAF Smart Quant Results

Element	Weight %	Atomic %	Net Int.	Net Int. Error
O K	38.5	81.61	166.44	0.01
BiM	42.62	6.92	166.15	0
FeK	18.88	11.47	41.16	0.06

REFERENCES

[1] A. Goldman, Handbook of Modern Ferromagnetic Materials, Norwell: Kluwer Academic Publishers, 1999.

[2] L. Tejuca, Properties and applications of perovskite-type oxides., New York: Marcel Dekker, Inc, 1993.

[3] Y. K. J. et al., "R3c-R3m Octahedron-tilting Transition in Rhombodedrally-distorted BiFeO3 Multiferroics," *Korean Physical Society,* vol. 58, no. 4, pp. 817-820, 2011.

[4] R. G. a. W. J. J. James R. Teague, "Dielectric Hysteresis In Single Crystal BiFeO3," *Solid State Communication,* vol. 8, no. 13, pp. 1073-1074, 1970.

[5] J. W. et al., "Epitaxial BiFeO3 Multiferroic Thin Film heterostructures," *Science,* vol. 299, no. 5613, pp. 1719-1722, 2003.

[6] B. Warren, X-Ray Diffraction, New York: Dover Publication, INC, 1990.

[7] "Nobelprize.org," [Online]. Available: http://www.nobelprize.org/nobel_prizes/physics/laureates/1915/. [Accessed 8 March 2013].

[8] N. D. M. Neil W. Ashcroft, "Solid State Physics," Belmont, CA, Brooks/Cole, 1976, pp. 96-108.

[9] "International Centre of Diffraction Data," [Online]. Available: http://www.icdd.com/. [Accessed 12 March 2013].

[10] "www.qdusa.com," Quantum Design,Inc., [Online]. Available: http://www.qdusa.com/sitedocs/appNotes/vsmappnote_5-09.pdf. [Accessed 12 March 2013].

[11] P. W. Peter Eaton, Atomic Force Microscopy, New York: Oxford University Press, 2010.

[12] T. H. Cunningham, "Quantitative Mobility Spectrum Analysis of III-V Heterostructures on Silicon," 2012.

[13] Z. Y. E. Ravi Droopad, "Development of integrated heterostructures on silicon by MBE," *Journal of Crystal Growth,* no. 251, pp. 638-644, 2003.

[14] J. F. S. Gustau Catalan, "Physics and Applications of Bismuth Ferrite," *Advanced Materials,* vol. 21, no. 24, pp. 2463-2485, 2009.

[15] S. G. P. D. R. K. J. Kabelac, "rf oxygen plasma assisted molecular beam epitaxy growth of BiFeO3 thin films on SrTiO3 (001)," *Vacuum Science and Technology,* vol. 25, no. 3, pp. 1049-1052, 2007.

[16] Y. K. K. H. F. S. K. Singh, "Epitaxial BiFeO3 thin films fabricated by chemical solution deposition," *Applied Physcis Letters,* vol. 88, no. 16, 2006.

[17] T. J. Z. M. O. L. L. L. F. Yan, "Role of Pb(Zr0.52Ti0.48)O3 substitution in multiferrroic properties of polycrystalline BiFeO3 thin films," *Journal of Applied Physics,* vol. 110, no. 11, 2011.

[18] J.-M. M. G. D. A. r. G. a. W. J. J. Christian Michel, "The Atomic Structure of BiFeO3," *Solid State Communications,* vol. 7, no. 9, pp. 701-704, 1969.

[19] W. E. et al., "Comment on Epitaxial BiFeO3 Multiferroic Thin Film Heterostructures," *Science,* vol. 307, no. 1203, 2005.

[20] J.-M. W. Y.-C. C. Y.-H. L. H.-N. L. Yi-Hsien Lee, "Surface Chemistry and Nanoscale Characteriations of Multiferroic BiFeO3 Thin Films," *Electrochemical and Solid-State Letters,* vol. 8, no. 10, 2005.

[21] S.-J. C. H.-y. L. S.-Y. C. Yen-Ting Liu, "Preperation of a BiFeO3/LaNiO3 multiferroic oside superlattice structure by RF magnetron sputtering," *Surface and Coating Technology,* vol. 206, no. 7, pp. 1666-1672, 2011.

[22] O. G. A. A. A. M.S. Kartavtseva, "BiFeO3 thin films prepared by MOCVD," *Surface and Coatings Technology,* vol. 201, no. 22-23, pp. 9149-9153, 2007.

VITA

Rye Alan Johnson was born in Corpus Christi, Texas on August 20, 1986, the son of Greg and Shelly Johnson. After completing his work at Memorial High School, Victoria, Texas, in 2004, he entered Texas State University-San Marcos. He finally received his degree of Bachelor of Science from Texas State in May 2010. In August 2010, he entered the Graduate College of Texas State.

Permanent E-mail Address: ryej86@gmail.com

This thesis was typed by Rye A. Johnson.